In vitro and in vivo synergistic effect of radiotherapy and plasmonic photothermal therapy on the viability of cancer cells using ^{177}Lu–Au-NLS-RGD-Aptamer nanoparticles under laser irradiation

Abraham González-Ruíz, Guillermina Ferro-Flores, Nallely Jiménez-Mancilla, et al.

Journal of Radioanalytical and Nuclear Chemistry
An International Journal Dealing with All Aspects and Applications of Nuclear Chemistry

ISSN 0236-5731
Volume 318
Number 3

J Radioanal Nucl Chem (2018)
318:1913-1921
DOI 10.1007/s10967-018-6266-6

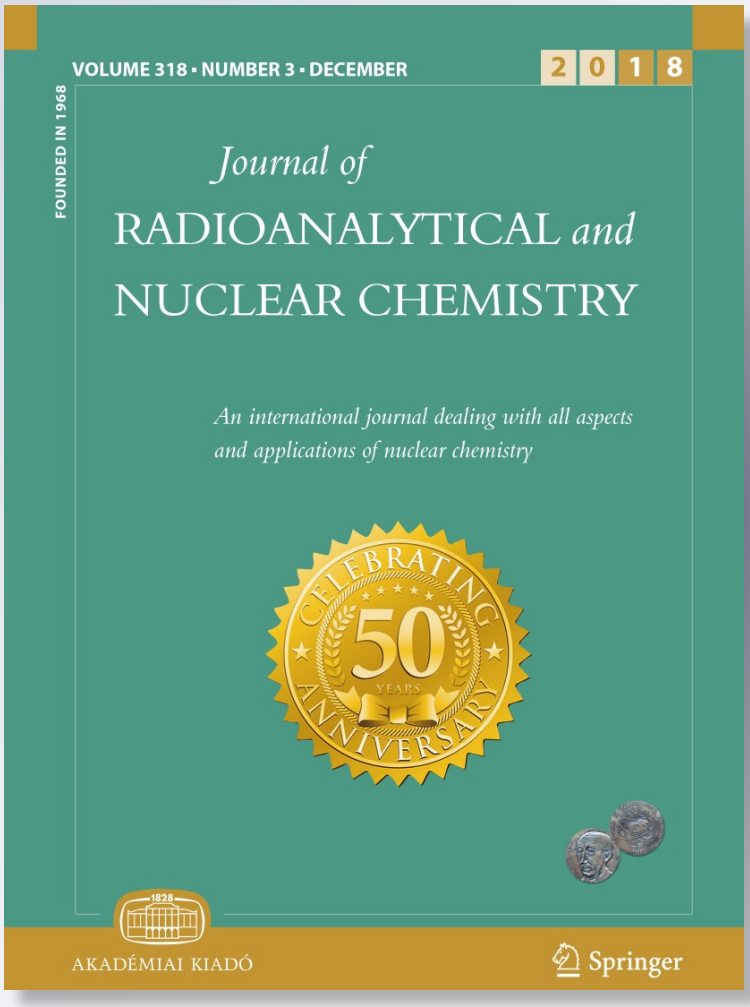

Springer

Journal of Radioanalytical and Nuclear Chemistry (2018) 318:1913–1921
https://doi.org/10.1007/s10967-018-6266-6

In vitro and in vivo synergistic effect of radiotherapy and plasmonic photothermal therapy on the viability of cancer cells using ^{177}Lu–Au-NLS-RGD-Aptamer nanoparticles under laser irradiation

Abraham González-Ruíz[1,2] · Guillermina Ferro-Flores[1] · Nallely Jiménez-Mancilla[2,3] · Alondra Escudero-Castellanos[1,2] · Blanca Ocampo-García[1] · Myrna Luna-Gutiérrez[1] · Clara Santos-Cuevas[1] · Enrique Morales-Avila[2] · Keila Isaac-Olivé[2]

Received: 24 June 2018 / Published online: 24 October 2018

Abstract

This research aimed to evaluate the photothermal and radiotherapeutic effect of the ^{177}Lu–Au-RGD-NLS-Aptamer anti-angiogenic nanosystem on the viability of U87MG cancer cells by using in vitro and in vivo models, as well as to assess the synergic effect of both therapies. In vitro results demonstrated a decrease in cell viability to 2.14 ± 0.27% after the treatment with photothermal therapy plus radiotherapy. These results correlated with the observed in vivo therapeutic response in mice with U87MG-induced tumors, in which ^{177}Lu–Au-RGD-NLS-Aptamer under laser irradiation inhibited tumor progression. The combination of radiotherapy and thermotherapy in one nanoradiopharmaceutical could be potentially useful for cancer treatment.

Keywords Lutetium-177 · ^{177}Lu–gold nanoparticles · Plasmonic photothermal therapy · Anti-VEGF aptamer · RGD peptide

Introduction

Radiopharmaceutical preparations based on ^{177}Lu-labeled gold nanoparticles are a relevant topic in the field of theranostic innovation for cancer management. Gold nanoparticles have a non-toxic nature, a surface of easy chemical functionalization and unique optical properties due to the SPR (surface plasmon resonance) effect [1]. Because of the SPR phenomenon, Au-nanoparticles have demonstrated to be a potential tool in plasmonic photothermal therapy [2, 3]. On the other hand, ^{177}Lu has been used in the design of multiple radiopharmaceuticals, due to its emitting radiation properties such as the therapeutic β_{max} emission of 0.497 MeV and its γ-radiation of 0.208 MeV for diagnostic imaging [4].

Current theranostic compounds aim to prevent tumor development from early stages. Inhibition of new vascular blood vessel formation around the tumor (angiogenesis) is crucial to inhibit the growth of the malignant lesion. Vascular endothelial growth factor (VEGF) and integrins overexpressed in the angiogenic process are potential inhibition targets to stop tumor development [5, 6].

^{177}Lu–Au nanoparticles have been effectively functionalized with peptides, antibodies or aptamers for specific binding to tumor receptors [7, 8]. Recently, we reported the synthesis and physicochemical characterization of the ^{177}Lu–Au-NLS-RGD-Aptamer system with fluorescence and anti-angiogenic properties by targeting both the VEGF pathway through the anti-VEGF aptamer, and the α(v)β(3) integrin through the NLS-RGD (Nuclear Localization Sequence-Arg-Gly-Asp) peptide [9]. Nevertheless, the ^{177}Lu–Au-nanoradiopharmaceutical could also allow the localized and simultaneous delivery of heat (by the SPR

✉ Guillermina Ferro-Flores
guillermina.ferro@inin.gob.mx;
ferro_flores@yahoo.com.mx

[1] Department of Radioactive Materials, Instituto Nacional de Investigaciones Nucleares, 52750 Ocoyoacac, Estado de México, Mexico

[2] Universidad Autónoma del Estado de México, 50180 Toluca, Estado de México, Mexico

[3] CONACyT, Instituto Nacional de Investigaciones Nucleares, 52750 Ocoyoacac, Estado de México, Mexico

effect) and ionizing radiation (by β-particle emission) near or inside the cell nucleus, generating a possible synergistic therapeutic effect between plasmonic photothermal therapy and radiotherapy [10].

This research aimed to evaluate the photothermal and radiotherapeutic effect of the ^{177}Lu–Au-NLS-RGD-Aptamer nanoradiopharmaceutical on the viability of U87MG cancer cells by using in vitro and in vivo models, as well as to assess the synergic effect of both therapies.

Experimental

Preparation of the ^{177}Lu–Au-nanosystems

The synthesis of both ^{177}Lu-labeled and unlabeled Au-nanosystem was described in a previous work [9]. Briefly, the DOTA-GGC (1,4,7,10-tetraazacyclododecane-N,N′,N″,N‴-tetraacetic acid-Gly-Gly-Cys) molecule was used as a ^{177}Lu (3 TBq/mg, 0.53 TBq/μmol, ITG, Germany) chelator, and for gold nanoparticles (20 nm, Sigma-Aldrich Co, USA) attachment, the conjugation through cysteine (active –SH group) was employed. Both molecules, NLS-RGD [NH_2-Gly-Arg-Lys–Lys-Arg–Arg-Gly–Gly-Cys-c(Arg-Gly-Asp-D-Tyr-Lys)-3-succinimidepropionylamide-Gly-Cys(Acm)-Gly-Cys(Acm)-$CONH_2$], and the anti-VEGF aptamer (28 RNA bases with the addition of a terminal pentyl-SH group, Iba Solutions Company, Germany), were also conjugated to the gold nanoparticle surface through the –SH group. In this research, the Au-conjugates were concentrated by ultracentrifugation (30,000 MW cut off, Amicon Ultracel, Millipore, USA) to 1.12×10^{13} nanoparticles/mL. For comparative purposes, the radioactive (^{177}Lu-DOTA-GGC-labeled) and non-radioactive nanoparticles of Au, Au-NLS-RGD, Au-Aptamer, and Au-NLS-RGD-Aptamer were also prepared. As previously reported, the number of RGD molecules is 16 while the number of Aptamer molecules is 27 per gold NP in the Au-nanosystems [9]. Therefore, the content of RGD/Aptamer ratio per gold NP in Au-NLS-RGD-Aptamer conjugate was 0.6. Detailed methods of radiolabeling and radiochemical purity assessment by ultrafiltration and size-exclusion chromatography have been shown elsewhere [11, 12].

The Au-NLS-RGD-Aptamer nanosystem was characterized by TEM (transmission electron microscopy) in shape and size (JEOL JEM2010 HT microscope operated at 200 kV) before and after laser irradiation. The nanoconjugate was also measured by UV–Vis spectroscopy (Perkin-Elmer Lambda-Bio spectrometer) to monitor the shift in the surface plasmon band before and after laser irradiation, as well as particle size analysis by DLS (Dynamic Light Scattering, Nanotrac Wave, USA). Radiochemical purity was also verified by ultrafiltration [12] after laser irradiation.

Cell culture

The U87MG rat glioma cell line was obtained from the American Type Culture Collection (Atlanta, GA, USA) and cultured (37 °C, 5% CO_2) in Roswell Park Memorial Institute Medium (Sigma-Aldrich Co.). Fetal bovine serum (10%), penicillin (100 U/mL) and streptomycin (100 μg/mL) were also used.

Induction of U87MG tumors in athymic mice

The studies of tumor uptake in mice were carried out according to that established in Official Mexican Norm 062-ZOO-1999. Athymic male mice (20–22 g) were kept in sterile cages with wood-shaving beds, constant temperature, humidity, noise and 12:12 light periods. By subcutaneous injection into the upper back of twenty 6–7-week-old nude mice, glioma tumors of U87MG cells (1.5×10^6 suspended in 0.2 mL of phosphate buffered saline) were induced.

Laser arrangement

An Nd-YAG laser (Qsmart-100, Quantel laser) pulsed for five ns at 532 nm (energy = 45.9 mJ/pulse) was used for the irradiation experiments with a repetition rate of 10 Hz. For the in vitro experiments, the irradiation time was 3.5 min (well plate area of 0.38 cm^2, ϕ 7 mm), and from 3.5 to 5.6 min for in vivo studies, due to the differences in tumor sizes throughout the study. A Dual-Channel Joulemeter/Power Meter (MolectronEPM 200, Coherent) was used for measurement of the power of each laser pulse. The laser covered the total well plate area as well as the tumoral area by using the diverging lens. The density of energy was in all cases 250 J/cm^2 (average irradiance of 1.19 W/cm^2). The well plate was placed over a heating plate at 37 °C (Microplate Thermo Shaker, HumanLab, China) during laser irradiation. The temperature measurements during in vitro experiments were carried out with a type-K thermocouple and an Arduino electronic circuit to process the data.

In vitro cell viability assay

U87MG cells suspended in fresh medium were incubated in a 96-well plate at a density of 1×10^4 cells/well for 24 h at 37 °C with 5% CO_2 and 85% humidity. For experimentation, culture media was removed, and cells were exposed to non-radioactive or radioactive Au-nanoparticles (Au-NLS-RGD-Aptamer, Au-NLS-RGD,

Au-Aptamer, Au, ^{177}Lu–Au-NLS-RGD-Aptamer, ^{177}Lu–Au-NLS-RGD, ^{177}Lu–Au-Aptamer or ^{177}Lu–Au) (100 μL, 1.12×10^{13} Au-nanoparticles). Untreated cells, $^{177}LuCl_3$ or laser irradiation of cells without Au-nanoparticles were considered as negative controls. The activity of radioactive compounds was 5 kBq/100 μL. For the evaluation of the thermotherapy effect, cells exposed to non-radioactive Au-nanosystems were irradiated with the laser. Cells exposed to ^{177}Lu–Au conjugates and irradiated with the laser were used for the evaluation of the synergistic effect between radiotherapy and thermotherapy. After 2 h of cell incubation with the non-radioactive or radioactive Au-nanoparticles and after laser irradiation, the solution in each well was removed and replaced with fresh culture media. Cells were maintained under standard culture conditions for 72 h. Finally, the viability of the cells was evaluated by standard XTT assay ((sodium 3′-[1-[phenylaminocarbonyl]-3,4-tetrazolium]-bis[4-methoxy-6-nitro]benzene sulfonic acid hydrate)). The absorbance of untreated cells was considered as 100% of living U87MG cells.

Therapeutic protocol

Four groups ($n = 4$) of athymic nude mice bearing U87MG gliomas (tumor size 0.05 ± 0.01 g) were used. Each group was subjected to one of the following treatments: (a) ^{177}Lu–Au-NLS-RGD-Aptamer (molecular radiotherapy), (b) Au-NLS-RGD-aptamer (laser irradiation: photothermal therapy) and (c) ^{177}Lu–Au-NLS-RGD-aptamer (molecular radiotherapy + laser irradiation: photothermal therapy). There was also an untreated control group. The injected activity was 2 MBq/0.05 mL, 5.6×10^{12} Au-nanoparticles/0.05 mL (injected intratumorally in mice under 2% isoflurane anesthesia). Cerenkov images were acquired at 96 h after intratumoral (i.t.) radiopharmaceutical injection (Xtreme/preclinical equipment, Bruker Corp., USA) to verify the ^{177}Lu–Au-NLS-RGD-Aptamer retention in tumors.

Each treatment was administered on days 1, 7, 14 and 21, for a total of four doses (radiotherapy and thermotherapy). The tumor irradiation was done with the same density of energy as the in vitro experiments (250 J/cm^2). Mice were kept under anesthesia (2% isoflurane) during the study. Tumor growth was verified weekly. The length (L) and width (a) were measured with calipers, and the volume was determined as $V = \pi/6 * (L)(a)^2$. The tumor mass was calculated considering a tumor density of 1 g/cm^3. After 25 days, the mice were sacrificed.

X-ray images (X-Treme preclinical equipment, Bruker Corp., USA) were acquired 3 d after the last injection (at 25 days of treatment). Mice kept under 2% isoflurane anesthesia were placed in the prone position, and imaging was performed.

Evaluation of the radiation absorbed dose

As a first step, in vivo biokinetics were obtained by dissection of mice ($n = 3$) with U87MG-induced tumors at 1, 3, 24. 48, 72, and 96 h after ^{177}Lu–Au-NLS-RGD–Aptamer (2 MBq/0.05 mL, 5.6×10^{12} Au-nanoparticles) intratumoral injection. This group was independent of the treatment groups previously mentioned. The extracted organs or tissue samples were measured using a NaI(Tl) detector (NML Laboratories Inc, USA) and results were expressed as a percentage of the injected activity per gram of tissue (% ID/g) or percentage of the injected activity per organ (%ID). Radioactivity of the main source regions (liver, spleen, kidneys, and tumor) as a function of time [Ah(t)] was adjusted to triexponential functions. As an evidence of the target-specific accumulation of the nanoradiopharmaceutical in tumors, a group of mice was previously injected (1 h before) with cold Au-NLS-RGD-Aptamer (1.12×10^{13}) to generate a receptor-blocking effect. Finally, mice were dissected 1 h after ^{177}Lu-nanosystem administration.

The $Ah(t)$ functions were used in the therapeutic protocol to obtain the total number of disintegrations (N) in the main source organs and tumor during the entire treatment (Eq. 1):

$$N_{\text{source}} = \int_{t=0}^{t=25\,\text{days}} Ah(t)\mathrm{d}t + \int_{t=7}^{t=25\,\text{days}} Ah(t)\mathrm{d}t + \int_{t=14}^{t=25\,\text{days}} Ah(t)\mathrm{d}t + \int_{t=21}^{t=25\,\text{days}} Ah(t)\mathrm{d}t \quad (1)$$

The radiation absorbed dose to organs and tumor was obtained according to Eq. 2:

$$\bar{D}_{\text{target}\leftarrow\text{source}} \sum_{\text{source}} N_{\text{source}} \times \text{DF}_{\text{target}\leftarrow\text{source}} \quad (2)$$

where $\bar{D}$ is the mean radiation absorbed dose and DF is a dose factor (Eq. 3):

$$\text{DF} = \frac{\sum n_i E_i \emptyset_i}{m} \quad (3)$$

DF values were calculated by using the organ masses (m) and absorbed energy fraction ($\emptyset_i$) reported for a mouse model by Miller et al. [13]. From the lutetium-177 beta spectrum, the $\sum n_i E_i$ was calculated.

Statistical analysis

The data are presented as mean ± SD of the results of three independent replicates of each condition tested. Three-way analysis of variance (ANOVA) was used to evaluate the effects of different treatments on cell viability. The differences between the in vivo treatments of the

unblocked and blocked receptors were assessed through Student's *t* test.

Results and discussion

Chemical results

TEM images and UV–Vis spectra of the Au-NLS-RGD-Aptamer before and after laser irradiation are shown in Fig. 1. As can be observed, the most significant change was a minimum increase in the aggregation factor (area under the curve between 600 and 700 nm). After ^{177}Lu–Au-NLS-RGD-Aptamer laser irradiation, the radiochemical purity remained stable (99%). These results confirmed that the laser treatment does not interfere with the stability of the nanoradiopharmaceutical, allowing the delivery of radiation doses until total radionuclide decay is achieved in the biological system.

In vitro photothermal and radiotherapeutic cytotoxicity of Au-nanosystems

Figure 2 shows the effect of the Au-NLS-RGD-Aptamer, Au-NLS-RGD, Au-Aptamer and Au nanoparticles on the temperature increase of the culture media containing U87MG cells and under laser irradiation at different times.

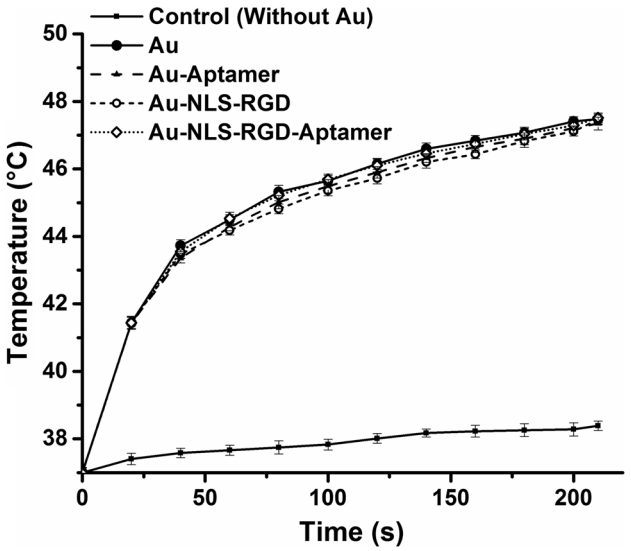

Fig. 2 Effect of the Au-NLS-RGD-Aptamer, Au-NLS-RGD, Au-Aptamer and Au nanoparticles on the temperature increase of the culture media containing U87MG cells and under laser irradiation at different times. Irradiation: Nd–YAG laser pulsed for 5 ns at 532 nm (energy = 45.9 mJ/pulse), repetition rate of 10 Hz

The temperature in each irradiated well reached ~ 47.5 °C (Δt = 10.5 °C) for all Au-nanoconjugates, exhibiting a significant difference ($p < 0.05$) with regard to the solution without any Au-nanoconjugate (control, Δt = 1.3 °C) (Fig. 2). This result was expected since, in all nanosystems,

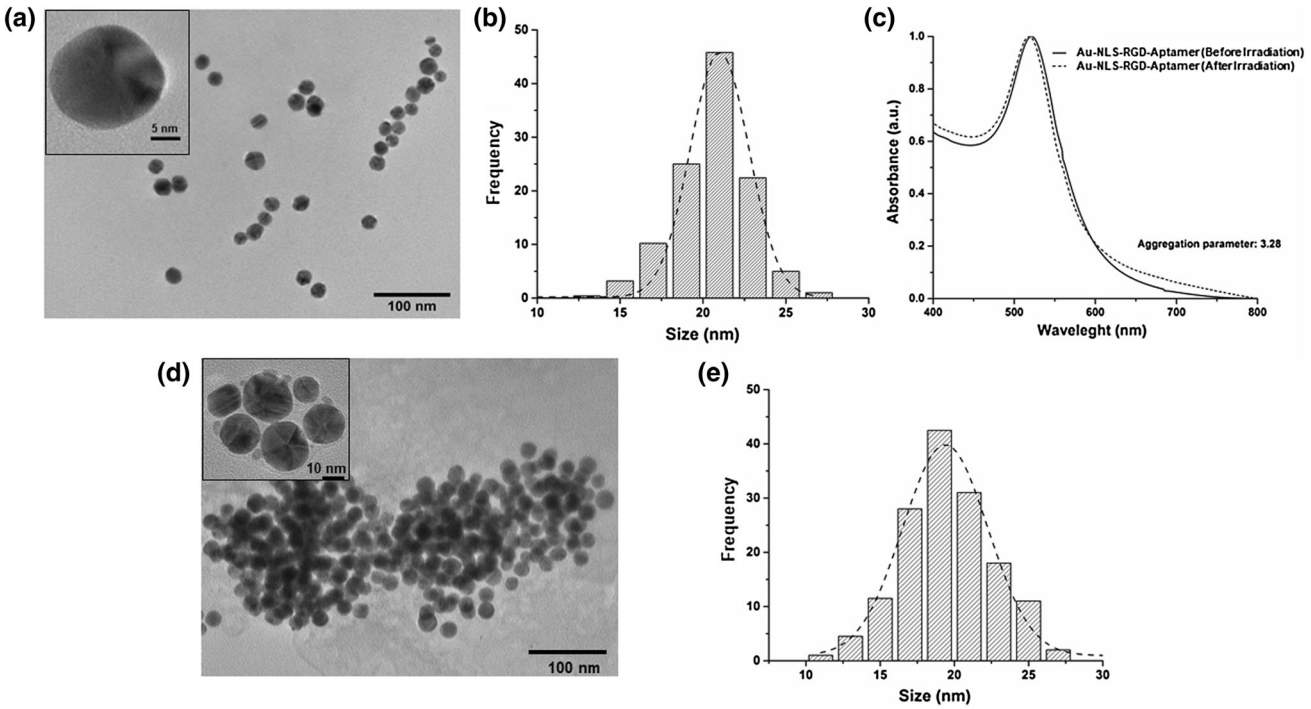

Fig. 1 Au-NLS-RGD-Aptamer nanosystem: TEM images **a** before and **d** after irradiation; particle size distribution **b** before and **e** after irradiation and **c** UV–Vis spectrum before and after irradiation. Irradiation: Nd–YAG laser pulsed for 5 ns at 532 nm (energy = 45.9 mJ/pulse), 3.5 min, repetition rate of 10 Hz (1.19 W/cm^2)

the laser beam interaction with gold nanoparticles causes the collective oscillation of electrons and light absorption that is converted to heat, delivered to the surrounding medium.

Figure 3 shows the viability assay results of the cells exposed to laser irradiation and/or targeted radiotherapy. ANOVA results indicate that all nanosystems had a significant effect ($p < 0.05$) on U87MG cell viability, with a statistically significant difference among the treatments. All Au–nanoconjugates under laser irradiation induced a significant ($p < 0.05$) loss of cell viability when compared to the cells irradiated without Au (control; cell viability > 88%), due to the localized heat deposition as a consequence of the SPR phenomenon. Likewise, all cells treated with ^{177}Lu–Au-nanosystems were significantly ($p < 0.05$) more affected in their viability that those treated with $^{177}LuCl_3$ (control; cell viability > 88%), due to the target–specific recognition and internalization of the nano-radiopharmaceuticals with the consequent radiation dose delivery inside cells. However, in agreement with our previous results, the Au-NLS-RGD-Aptamer system produced the most significant effect over U87MG cancer cell viability because of the higher cell uptake and internalization with regard to those of Au-NLS-RGD and Au-Aptamer nanoconjugates [9].

Additionally, the affinity of the Aptamer (anti-VEGF), RGD (by the integrins α(v)β(3) over-expressed in U87MG cells), and the nuclear localization properties of the NLS sequence, allow a higher uptake and accumulation of the Au-NLS-RGD-Aptamer near and inside the cell nucleus. It is known from theoretical studies, that temperature reaches 700 °C around a 20 nm-spherical gold nanoparticle when it is under laser irradiation (530 nm) [14]. Therefore, the localized delivery of heat and ionizing radiation near or inside cell nucleus during the ^{177}Lu–Au-NLS-RGD-Aptamer plus the irradiation treatment causes the most U87MG cell damage (Fig. 3). The significant ($p < 0.05$) synergistic effect of the plasmonic photothermal therapy (thermotherapy) and the targeted radiotherapy on cell viability in all treatments with regard to the single treatment (thermotherapy or radiotherapy) is also evident in Fig. 3. It is important to emphasize that the main feature of ionizing radiation is the localized release of large amounts of energy, which is more than enough to break a chemical bond; therefore, the biologic radiation effects result principally from direct and indirect damage to DNA. Since proteins are the primary target for thermal cell damage [15], the two therapies (photothermal therapy and targeted radiotherapy), with different mechanisms to produce cell damage, resulted in an additive ability to kill tumor cells when they were used simultaneously. Other differences between irradiation (radiation therapy) and heating (thermotherapy) at the immuno-molecular level, recently reported by Finkel et al. [16] and Werthmöller et al. [17], also support the aforementioned synergistic effect.

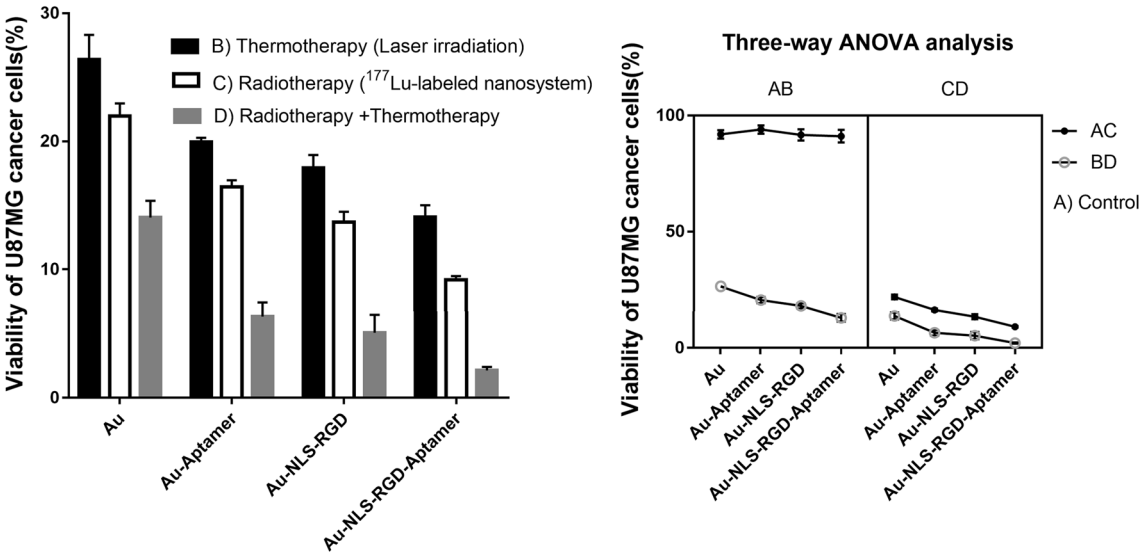

Fig. 3 Left: effect on the viability of U87MG cells exposed to (B) Au-NLS-RGD-Aptamer, Au-NLS-RGD, Au-Aptamer and Au nanoparticles under laser irradiation (thermotherapy, Nd-YAG laser, 532 nm); or (C) ^{177}Lu–Au-NLS-RGD-Aptamer, ^{177}Lu–Au-NLS-RGD, ^{177}Lu–Au-Aptamer and ^{177}Lu–Au nanosystems (targeted radiotherapy); or (D) ^{177}Lu–Au-NLS-RGD-Aptamer, ^{177}Lu–Au-NLS-RGD, ^{177}Lu–Au-Aptamer, and ^{177}Lu–Au nanosystems under laser irradiation (targeted radiotherapy plus thermotherapy). Right: graphical representation of the three-way ANOVA analysis of the (B), (C) and (D) treatments. (A) Negative controls ($^{177}LuCl_3$ or U87MG cells irradiated without Au-nanoparticles)

In vivo therapeutic protocol

Biodistribution studies showed that 38.42 ± 3.35% of the ^{177}Lu–Au-NLS-RGD-Aptamer remains in the tumor at 96 h after i.t. administration (Table 1).

It was confirmed with the Cerenkov images acquired at 96 h post-radiopharmaceutical injection, in which the activity (Cerenkov light produced from β-particles of ^{177}Lu in tissue) associated to the tumor is clearly visible as result of the high radiopharmaceutical retention (Fig. 4).

Liver, spleen, and kidney had a remarkably lower uptake after 96 h (< 0.7% ID) compared to that of the tumor (38.4% ID), and that is why they were not visible in the Cerenkov imaging modality. The overall specificity was confirmed by the partial receptor blocking study, in which a previous injection of the non-radioactive Au-NLS-RGD-Aptamer significantly reduced (*t*-student test, $p < 0.05$) the activity of tumors. Nevertheless, at 1 h, a high percentage of the administered activity remained in the blocked tumor (75.19% for the unblocked tissue vs. 33.25% in the blocked tissue) due to the passive accumulation of the nanosystem in the tumoral lesion, induced by its colloidal nature and by the well-known passive EPR (enhanced permeability and retention) effect [18]. Passive targeting in the tumors occurred due to extravasations through leaky blood vessels (gaps—100–600 nm), but the significant difference in tumor uptake (20.06%) is related to active targeting, which means a target-specific recognition. Biokinetic models also indicated that the total number of disintegrations and average absorbed radiation dose are significantly higher in the tumor than the other source organs (Table 2).

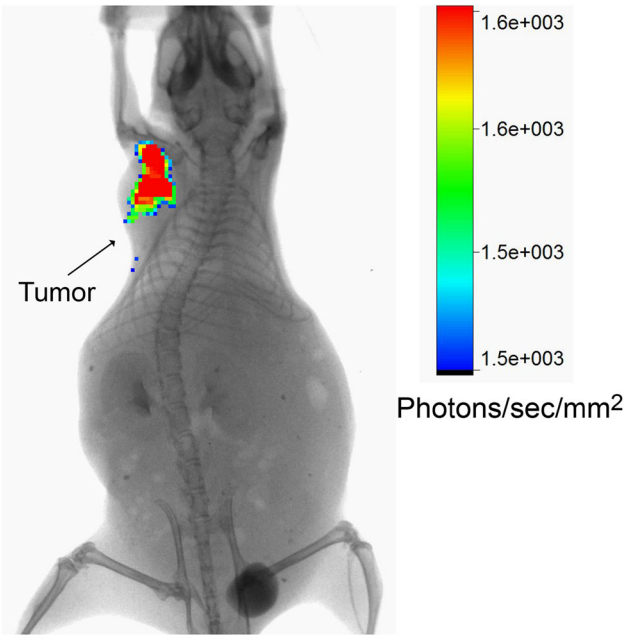

Fig. 4 Cerenkov image (X-treme/preclinical equipment) acquired at 96 h after intratumoral administration of the ^{177}Lu–Au-NLS-RGD-Aptamer nanosystem. The activity (Cerenkov light produced from β^- particles of ^{177}Lu in tissue) associated to the tumor is clearly visible as result of the high radiopharmaceutical retention

ANOVA results of the in vivo studies demonstrated that there is a statistically significant difference ($p < 0.05$) in all treatments. The progression of tumor size for the Au–

Table 1 Biodistribution in mice with U87MG-induced tumors after intratumoral administration of ^{177}Lu–Au-NLS-RGD-Aptamer nanoparticles, expressed as a percentage of the injected dose/g of tissue (% ID/g^{++}) or a percentage of the injected dose per organ (% ID^{+}) (mean ± SD, $n = 3$)

Tissue	Unblocked						Blocked[a]
	1 h	3 h	24 h	48 h	72 h	96 h	1 h
Blood^{++}	0.22 ± 0.03*	0.19 ± 0.03	0.07 ± 0.04	0.01 ± 0.01	0.01 ± 0.01	0.00 ± 0.00	1.95 ± 0.76*
Heart^{+}	0.16 ± 0.08	0.08 ± 0.05	0.00 ± 0.00	0.00 ± 0.00	0.00 ± 0.00	0.00 ± 0.00	1.11 ± 0.35
Lung^{+}	0.32 ± 0.08	0.18 ± 0.03	0.08 ± 0.03	0.00 ± 0.00	0.00 ± 0.00	0.00 ± 0.00	1.09 ± 0.28
Liver^{+}	1.98 ± 0.23*	2.15 ± 0.12	0.91 ± 0.39	0.82 ± 0.12	0.75 ± 0.11	0.51 ± 0.12	4.03 ± 0.95*
Pancreas^{+}	0.12 ± 0.07	0.10 ± 0.06	0.08 ± 0.02	0.02 ± 0.01	0.00 ± 0.00	0.00 ± 0.00	0.11 ± 0.04
Spleen^{+}	0.62 ± 0.13	1.20 ± 0.12	0.64 ± 0.38	0.38 ± 0.15	0.19 ± 0.07	0.16 ± 0.21	0.32 ± 0.29
Kidneys^{+}	2.57 ± 0.38*	3.87 ± 0.95	1.79 ± 0.89	1.03 ± 0.25	0.79 ± 0.13	0.67 ± 0.12	5.57 ± 1.14*
Intestine^{++}	0.54 ± 0.14	0.49 ± 0.09	0.31 ± 0.18	0.18 ± 0.10	0.08 ± 0.03	0.04 ± 0.02	0.32 ± 0.18
Muscle^{++}	0.11 ± 0.03	0.06 ± 0.03	0.00 ± 0.00	0.00 ± 0.00	0.00 ± 0.00	0.00 ± 0.00	0.21 ± 0.10
Bone^{++}	0.14 ± 0.02	0.02 ± 0.02	0.00 ± 0.00	0.00 ± 0.00	0.00 ± 0.00	0.00 ± 0.00	0.27 ± 0.15
U87MG Tumor^{+}	75.19 ± 5.12*	58.31 ± 4.21	53.52 ± 5.07	43.23 ± 4.32	39.92 ± 4.08	38.42 ± 3.35	33.25 ± 4.15*

*Significant difference ($p < 0.05$) between unblocked and blocked cell receptors

[a]Blocked with an additional intratumoral cold Au-NLS-RGD-Aptamer nanoparticle blocking dose 1 h prior to administration of ^{177}Lu Au-NLS-RGD-Aptamer, in order to determine the non-specific binding of the radioactivity

Table 2 Biokinetic models and average radiation absorbed doses of the principal source organs of mice with U87MG-induced tumors after intratumoral administration of ^{177}Lu–Au-NLS-RGD-Aptamer

Organ	Biokinetic model	N_{total} (MBq * h/MBq) (four injections at different times)	Average radiation absorbed dose (Gy/MBq)
Kidney	$A_h(t) = -7.42e^{-1.434t} + 3.57e^{-0.062t} + 0.98e^{-0.008t}$	1.31	0.39
Liver	$A_h(t) = -14.60e^{-2.604t} + 2.67e^{-0.308t} + 1.10e^{-0.011t}$	0.58	0.04
Spleen	$A_h(t) = -4.51e^{-1.914t} + 1.18e^{-0.039t} + 0.15e^{-0.008t}$	0.44	0.36
Tumor	$A_h(t) = 34.80e^{-1.484t} + 43.20e^{-1.534t} + 58.11e^{-0.009t}$	29.84	89

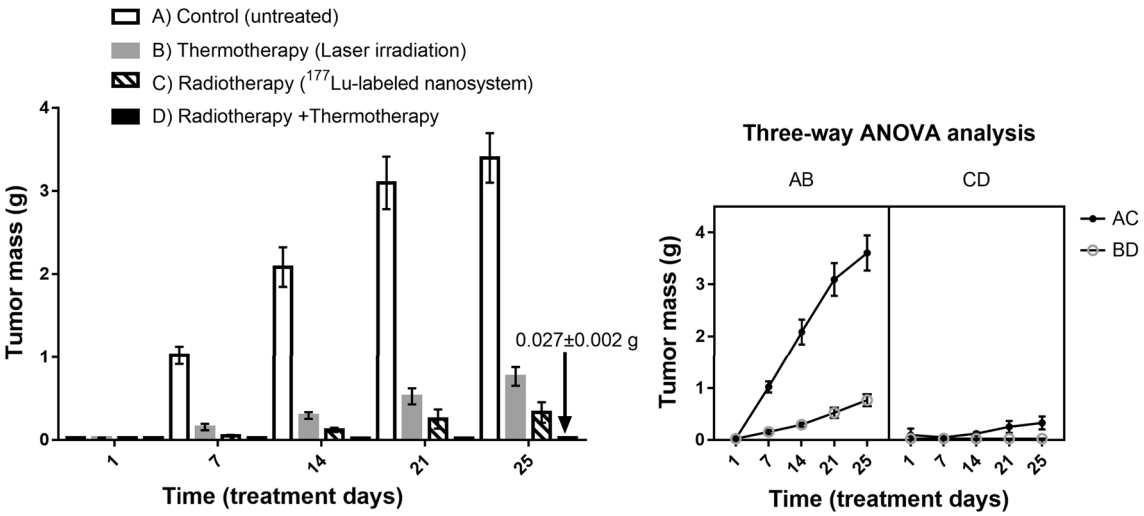

Fig. 5 Left: Tumor size progression for (B) Thermotherapy (Au-NLS-RGD-Aptamer under laser irradiation), (C) Targeted radiotherapy (^{177}Lu–Au-NLS-RGD-Aptamer), and (D) Thermotherapy plus radiotherapy (^{177}Lu–Au-NLS-RGD-Aptamer under laser irradiation) groups at different days of the treatment. Right: graphical representation of the three-way ANOVA analysis of the (A) control (untreated) and B, C, and D treatments

nanoconjugates was significantly lower ($p < 0.05$) after 25 days compared to that of the control group (Fig. 5). At 25 days, the tumor size in the ^{177}Lu-labeled Au-NLS-RGD-Aptamer nanosystem group under laser irradiation (radiotherapy plus thermotherapy) was 126 times smaller than that of the controls, and 28 times and 12 times lower than in the thermotherapy and radiotherapy groups, respectively (Fig. 5). The average radiation absorbed doses in tumors at the end of the radiotherapy treatment were 80 Gy for the ^{177}Lu–AuNP-NLS-RGD-Aptamer and 89 Gy in the case of ^{177}Lu–AuNP-NLS-RGD-Aptamer plus laser irradiation. Differences in the radiation absorbed doses for the same radiopharmaceutical are associated with a significantly ($p < 0.05$) greater progression of the tumor mass when radiotherapy was performed without thermotherapy (0.329 ± 0.124 g for the single treatment vs. 0.027 ± 0.002 g for the dual therapy).

Radiotherapy results are in agreement with those reported by Vilchis-Juarez et al. [12], using different ^{177}Lu-radiopharmaceuticals in the treatment of C6 glioma tumors in mice, but improved in this research by adding the plasmonic photothermal therapy. Figure 6 shows the X-ray images at 96 h after the last injection (at 25 days of treatment), in which the significantly smaller size of the tumor, due the synergistic effect of the photothermal and radiotherapy treatment, can be observed when compared to the results of the single procedures and the control (untreated). It is well-known that hyperthermia increases the effectiveness of radiation therapy by improving tumor oxygenation and affecting DNA repair mechanisms [15]. Furthermore, tumor hypoxia does not protect cells from heat as it does from ionizing radiation. Conversely, hyperthermia is effective at reversing hypoxia through the increase of vascular perfusion. Therefore, radiosensitization by hyperthermia is a critical mechanism induced in the synergistic effect observed in this research. Nevertheless, immune sensitization by heat has also been reported as a possible tool for cancer treatment, since hyperthermia affects multiple aspects of the antitumor immune system [19, 20].

For potential clinical applications, the ^{177}Lu–Au-NLS-RGD-Aptamer radiopharmaceutical prepared in this study could also be used in photothermal therapy by using short NIR (near infrared) laser pulses to generate a second

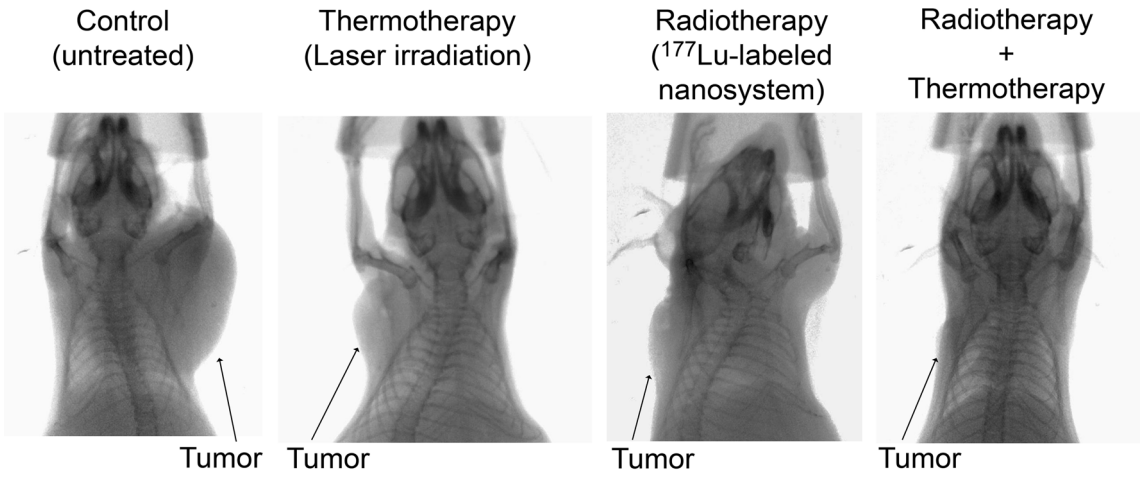

Fig. 6 X-ray images (X-Treme/preclinical equipment) of mice with U87MG tumors under thermotherapy (Au-NLS-RGD-Aptamer under laser irradiation), targeted radiotherapy (^{177}Lu–Au-NLS-RGD-Aptamer) and thermotherapy plus radiotherapy (^{177}Lu–Au-NLS-RGD-Aptamer under laser irradiation) treatments at 96 h after the last injection (at 25 days of treatment)

harmonic, which converts the NIR photons (800 nm) to visible photons (400 nm). The visible photons can be absorbed by the ^{177}Lu-nanospheres through SPR and electron interband transition with the conversion of their energy into heat [21]. The use of NIR light is important because tissues in the body are moderately transparent to NIR photons, thus creating the possibility of producing therapeutic effects in deep tissues [10, 21].

Although several articles have used iron oxide and gold nanoparticles for in vivo thermotherapy [22–24], this is the first time that target-specific radiolabeled gold nanoparticles are reported as novel nanosystems that efficiently combine the therapeutic properties of radiotherapy and hyperthermia as a synergistic modality in vivo. Nevertheless, ^{177}Lu–Au-NLS-RGD-Aptamer-anti-VEGF under laser irradiation must be evaluated in different cancer cells both in vitro and in vivo, as well as its effect on long-term cell proliferation to establish its clinical potential.

Conclusions

Due to the synergistic effect of its photothermal and radiotherapeutic properties, the ^{177}Lu–Au-RGD-NLS-Aptamer nanoradiopharmaceutical produced a significant ($p < 0.05$) in vitro and in vivo decrease in U87MG cell viability. Furthermore, the nanosystem inhibited tumor progression. The combination of radiotherapy and thermotherapy in one nanoradiopharmaceutical under laser irradiation could be potentially useful in cancer treatment.

Acknowledgements This research received financial support from the Mexican National Council of Science and Technology (CONACyT-Mexico, Grant 242443). This work was performed as part of the activities of the "Laboratorio Nacional de Investigación y Desarrollo de Radiofármacos, CONACyT".

Compliance with ethical standards

Conflict of interest The authors declare no potential conflict of interest with regard to the research, authorship, and/or publication of this article.

Ethical approval All applicable international, national, and/or institutional guidelines for the care and use of animals were followed.

References

1. Zarschler K, Rocks L, Licciardello N et al (2016) Ultrasmall inorganic nanoparticles: state-of-the-art and perspectives for biomedical applications. Nanomedicine 12:1663–1701. https://doi.org/10.1016/j.nano.2016.02.019
2. Elbialy N, Abdelhamid M, Youssef T (2010) Low power argon laser-induced thermal therapy for subcutaneous Ehrlich carcinoma in mice using spherical gold nanoparticles. J Biomed Nanotechnol 6:687–693. https://doi.org/10.1166/jbn.2010.1166
3. Abadeer NS, Murphy CJ (2016) Recent progress in cancer thermal therapy using gold nanoparticles. J Phys Chem C 120:4691–4716. https://doi.org/10.1021/acs.jpcc.5b11232
4. Banerjee S, Pillai M, Knapp F (2015) Lutetium-177 therapeutic radiopharmaceuticals: linking chemistry, radiochemistry, and practical applications. Chem Rev 115:2934–2974. https://doi.org/10.1021/cr500171e
5. Frezzetti D, Gallo M (2016) Vascular endothelial growth factor A regulates the secretion of different angiogenic factors in lung cancer cells. J Cell Physiol 231:1514–1521. https://doi.org/10.1002/jcp.25243
6. Ellert-Miklaszewska A, Poleszak K, Kaminska B (2017) Short peptides interfering with signaling pathways as new therapeutic tools for cancer treatment. Future Med Chem 9:199–221. https://doi.org/10.4155/fmc-2016-0189
7. Ferro-Flores G, Ocampo-Garcia BE, Santos-Cuevas CL et al (2015) Theranostic radiopharmaceuticals based on gold nanoparticles labeled with (177)Lu and conjugated to peptides.

Curr Radiopharm 8:150–159. https://doi.org/10.2174/1874471008666150313115423
8. Yook S, Cai Z, Lu Y, Winnik MA, Pignol J, Reilly RM (2015) Radiation nanomedicine for EGFR-positive breast cancer: panitumumab-modified gold nanoparticles complexed to the β-particle-emitter. (177)Lu. Mol Pharm 12:3963–3972. https://doi.org/10.1021/acs.molpharmaceut.5b00425
9. Gonzalez-Ruiz A, Ferro-Flores G, Azorín-Vega E et al (2017) Synthesis and in vitro evaluation of an antiangiogenic cancer-specific dual-targeting ^{177}Lu–Au-nanoradiopharmaceutical. J Radioanal Nucl Chem 314:1337–1345. https://doi.org/10.1007/s10967-017-5465-x
10. Jimenez-Mancilla N, Ferro-Flores G, Santos-Cuevas CL et al (2013) Multifunctional targeted therapy system based on 99mTc/^{177}Lu-labeled gold nanoparticles-Tat (49–57)-Lys3-bombesin internalized in nuclei of prostate cancer cells. J Label Compd Radiopharm 56:663–671. https://doi.org/10.1002/jlcr.3087
11. Morales-Avila E, Ferro-Flores G, Ocampo-García BE et al (2011) Multimeric system of 99mTc-labeled gold nanoparticles conjugated to c[RGDfK(C)] for molecular imaging of tumor alpha(v)beta(3) expression. Bioconjug Chem 22:913–922. https://doi.org/10.1021/bc100551s
12. Vilchis-Juarez A, Ferro-Flores G, Santos-Cuevas C et al (2014) Molecular targeting radiotherapy with cyclo-RGDfK(C) peptides conjugated to ^{177}Lu-labeled gold nanoparticles in tumor-bearing mice. J Biomed Nanotechnol 10:393–404. https://doi.org/10.1166/jbn.2014.1721
13. Miller WH, Hartmann-Siantar C, Fisher D et al (2005) Evaluation of beta-absorbed fractions in a mouse model for ^{90}Y, ^{188}Re, ^{166}Ho, ^{149}Pm, ^{64}Cu, and ^{177}Lu radionuclides. Cancer Biother Radiopharm 20:436–449. https://doi.org/10.1089/cbr.2005.20.436
14. Letfullin RR, Iversen CB, George TF (2011) Modeling nanophotothermal therapy: kinetics of thermal ablation of healthy and cancerous cell organelles and gold nanoparticles. Nanomedicine 7:137–145. https://doi.org/10.1016/j.nano.2010.06.011
15. Hall EJ, Giaccia AJ (2012) Radiobiology for the radiologist. Wolters Kluwer Health/Lippincott Williams & Wilkins, Philadelphia
16. Finkel P, Frey B, Mayer F et al (2016) The dual role of NK cells in antitumor reactions triggered by ionizing radiation in combination with hyperthermia. Oncoimmunology 5(6):e1101206. https://doi.org/10.1080/2162402X.2015.1101206
17. Werthmöller N, Frey B, Rückert M et al (2016) Combination of ionising radiation with hyperthermia increases the immunogenic potential of B16-F10 melanoma cells in vitro and in vivo. Int J Hyperth 32:23–30. https://doi.org/10.3109/02656736.2015.1106011
18. Maeda A, Wu J, Sawa T et al (2000) Tumor vascular permeability and the EPR effect in macromolecular thearpeutics: a review. J Control Release 65:271–284. https://doi.org/10.1016/S0168-3659(99)00248-5
19. Peer AJ, Grimm MJ, Zynda ER et al (2010) Diverse immune mechanisms may contribute to the survival benefit seen in cancer patients receiving hyperthermia. Immunol Res 46:137–154. https://doi.org/10.1007/s12026-009-8115-8
20. Zhang Y, Li N, Suh H et al (2018) Nanoparticle anchoring targets immune agonists to tumors enabling anti-cancer immunity without systemic toxicity. Nat Commun 9:6. https://doi.org/10.1038/s41467-017-02251-3
21. Huang X, Qian W, El-Sayed IH et al (2007) The potential use of the enhanced nonlinear properties of gold nanospheres in photothermal cancer therapy. Lasers Surg Med 39:747–753. https://doi.org/10.1002/lsm.20577
22. Espinosa A, Bugnet M, Radtke G et al (2015) Can magneto-plasmonic nanohybrids efficiently combine photothermia with magnetic hyperthermia? Nanoscale 7:18872–18877. https://doi.org/10.1039/c5nr06168g
23. Luna-Gutierrez M, Ferro-Flores G, Ocampo-Garcia BE et al (2013) A therapeutic system of ^{177}Lu-labeled gold nanoparticles-RGD internalized in breast cancer cells. J Mex Chem Soc 57:212–219
24. Sabale S, Kandesar P, Jadhav V et al (2017) Recent developments in the synthesis, properties, and biomedical applications of core/shell superparamagnetic iron oxide nanoparticles with gold. Biomater Sci 5:2212–2225. https://doi.org/10.1039/c7bm00723j